Role of hubs in outbreaks of cooperative contagions

Yongjoo Baek,[1] Kihong Chung,[2, 3] Meesoon Ha,[4, *] Hawoong Jeong,[5] and Daniel Kim[2, 6]

[1]*DAMTP, Centre for Mathematical Sciences, University of Cambridge, Cambridge CB3 0WA, United Kingdom*
[2]*Natural Science Research Institute, Korea Advanced Institute of Science and Technology, Daejeon 34141, Korea*
[3]*Samsung Semiconductor R&D Center, Hwaseong 18448, Korea*
[4]*Department of Physics Education, Chosun University, Gwangju 61452, Korea*
[5]*Department of Physics and Institute for the BioCentury,*
Korea Advanced Institute of Science and Technology, Daejeon 34141, Korea
[6]*Samsung SDS, Seoul 05510, Korea*
(Dated: October 1, 2018)

Social contagions have two major features: the cooperation among spreaders and the dominance of hubs. By exactly solving the generalized epidemic process on random scale-free networks with the power-law degree distribution $p_k \sim k^{-\alpha}$, we clarify how the interplay between the two features affects the transition between endemic and epidemic phases. Our results show that, even if cooperation requires a large number of infected neighbors, for $\alpha < 4$ the hubs can still induce distinctive cooperative phenomena, namely mixed-order transitions with the characteristics of both continuous and discontinuous transitions. We also find that for $2 < \alpha < 3$ an epidemic outbreak is possible purely through cooperative infections of hubs. The changing role of hubs is manifest in the nonmonotonic behaviors of the crossover exponent in the vicinity of the tricritical point.

There has been a growing body of literature on the *mixed-order transitions* (MOTs), which qualify as both continuous and discontinuous phase transitions depending on the chosen order parameter. Such transitions appear in many different contexts, such as DNA unzipping [1, 2], Ising spins with long-range interactions [3], and various percolation models with the biased merging of clusters [4]. A common aspect of these systems is the existence of long-range interactions, which enhances the probability of a large-scale avalanche over a finite fraction of the system at criticality [5].

Recently added to the list are the epidemic models of *cooperative contagions* [6–24], in which the probability of infection (or transmission) changes according to the number of other spreaders sharing the same target. Such mechanisms are at work in the adoption of new behaviors [25] and the cooperative co-infections [26, 27]. For *simple contagions*, in which every infection occurs independently, it is well known that the transition between the endemic and the epidemic phases is purely continuous [28]. In contrast, with sufficient boost from cooperations, in cooperative contagions the transition can be a MOT: a continuous transition of the outbreak probability coincides with a discontinuous jump of the outbreak size [10–24]. Moreover, the lines of MOTs and purely continuous transitions join at a tricritical point (TCP) with its own critical properties [29]. As in the other examples, the long loops of the underlying substrate, which facilitate the crossing of different infection pathways at criticality, plays a crucial role in the large-scale avalanches producing the discontinuous jump [16–18].

A natural question is how the conditions for the MOTs depend on the structure of the underlying substrate.

Most studies have addressed the question in homogeneous structures, such as lattices [10–13, 17, 22] and Poissonian random networks [8–10, 15–23], where a MOT requires a sufficiently strong boost from the cooperation of two neighbors [8–10]. However, contagions typically occur on heterogeneous structures: for instance, social networks feature a significant fraction of highly-connected individuals called *hubs*, whose existence is typically modeled by *scale-free networks* (SFNs) with a power-law distribution $p_k \sim k^{-\alpha}$ of the number of neighbors k (called *degree*) [30, 31]. Since the large variance of k in the SFNs leads to a large number of loops [32], it is natural to expect that the interplay of cooperativity and hubs is a crucial factor determining the transition behaviors of cooperative social contagions.

In this study, we show that an abundance of hubs facilitate MOTs, even if cooperation takes effect only with an arbitrarily large number of infected neighbors. To this end, we study the generalized epidemic process (GEP), in which the probability of infection depends on how many other neighbors have unsuccessfully tried to infect the target individual [10]. The model has been studied on lattices [10–13] and Poissonian [10, 15] or modular random networks [14], with the simplifying assumption that the infection probability changes at the second attempt. We introduce the general *cooperation threshold* $n \geq 2$ so that the infection probability changes at the n-th attempt. Based on the exact solution of the GEP and its near-TCP behaviors for different values of α and n, we clarify the role of the hubs in the endemic-to-epidemic phase transitions.

Dynamics. — In the GEP, a node can be susceptible ($\mathbf{S_1}$), weakened ($\mathbf{S_2}$), infected ($\mathbf{I}$), or removed ($\mathbf{R}$). All nodes are initially $\mathbf{S_1}$, except for one randomly chosen $\mathbf{I}$-node (the "seed") starting the contagion. At each time step, a random $\mathbf{I}$-node attempts to infect all of its $\mathbf{S_1}$- or $\mathbf{S_2}$-neighbors, each of the former (latter) with probability
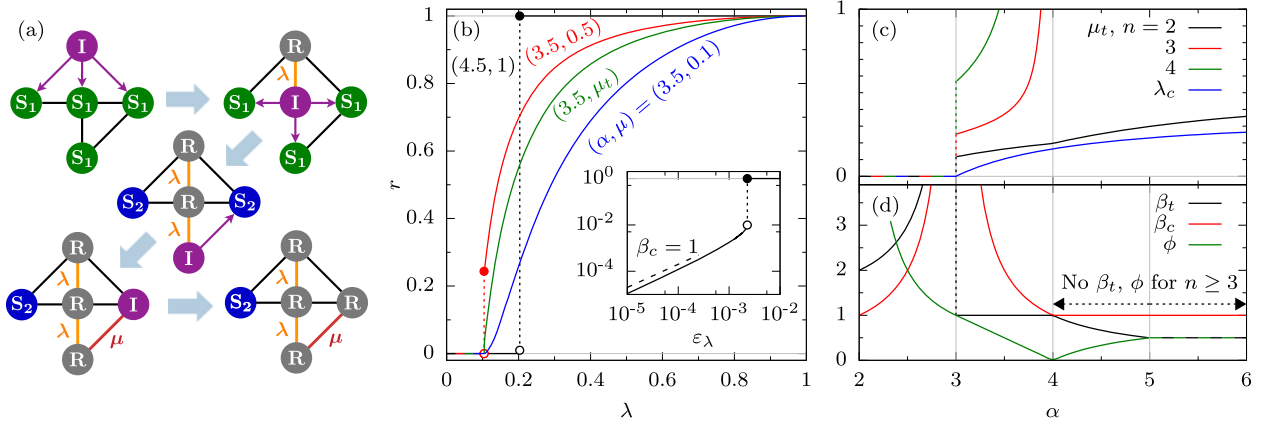
FIG. 1. (a) The GEP with $n = 3$ on a five-node network. Each thick arrow represents a time step. (b) Examples of the transitions of r in the GEP with $n = 3$ on the SFNs. Inset: a magnified view of the double phase transition for $(\alpha, \mu) = (4.5, 1)$. (c) The α-dependence of the TCP (λ_c, μ_t) and (d) the scaling exponents in Table I. The SFNs in (b)–(d) have $k_m = 4$ (see Eq. (1)).

λ (μ). Upon success, the target becomes **I**. A failed attempt does not affect the target unless it is the $(n-1)$-th attempt on the same **S₁**-node, in which case the node becomes **S₂**. After then, the attacking **I**-node immediately deactivates and becomes **R**, permanently removing itself from the dynamics. The process goes on until the network runs out of **I**-nodes. The final fraction of **R**-nodes, denoted by r, quantifies the outbreak size. As a simple example, the GEP with $n = 3$ on a five-node network is illustrated in Fig. 1(a).

Substrate. — The GEP spreads on an ensemble of infinitely large random SFNs constrained by two conditions. First, the degree distribution obeys a power law

$$p_k = k^{-\alpha}/\zeta_{\alpha,k_m} \quad \text{for } k \geq k_m \text{ and } \alpha > 2, \qquad (1)$$

where the generalized zeta function $\zeta_{s,v}$, defined as the analytic continuation of $\sum_{i=v}^{\infty} k^{-s}$ for $s \neq 1$, normalizes the distribution. The assumed range of α ensures that the mean degree $\langle k \rangle = \zeta_{\alpha-1,k_m}/\zeta_{\alpha,k_m}$ is finite and that the network is *locally tree-like* with negligible short loops [33]. Second, there is no correlation between the degrees of adjacent nodes. These two conditions guarantee that a node and each of its neighbors have mutually independent statistics, based on which one can exactly calculate the transition behaviors of r.

Transition of outbreak probability. — First, we discuss the transition of the probability P_∞ that an epidemic outbreak with $r > 0$ occurs. On locally tree-like networks, multiple infection pathways rarely cross at the same node unless the contagion has already spread to a finite fraction of the network. For this reason, μ is completely irrelevant to the transition from $P_\infty = 0$ to $P_\infty > 0$: only λ controls the transition by a bond-percolation mechanism. Thus one can simply apply the theory of bond percolation on the random SFNs [34, 35] to obtain the

transition point (or the *epidemic threshold*)

$$\lambda_c = \begin{cases} \frac{\langle k \rangle}{\langle k(k-1) \rangle} = \frac{\zeta_{\alpha-1,k_m}}{\zeta_{\alpha-2,k_m} - \zeta_{\alpha-1,k_m}} & \text{for } \alpha > 3, \\ 0 & \text{for } 2 < \alpha < 3, \end{cases} \qquad (2)$$

which lies between 0 and 1 for sufficiently large k_m. The percolation theory [36] also shows that the transition can only be continuous with the universal scaling behavior $P_\infty \sim \epsilon_\lambda^{\beta_c}$ for small positive $\epsilon_\lambda \equiv (\lambda - \lambda_c)/\lambda_c$, where the α-dependent values of the critical exponent β_c are listed in Table I. Such equivalence has also been noted for the GEP [10, 15] and other similar cooperative contagions [16–21] on homogeneous networks.

Exact outbreak size. — In contrast to P_∞, the outbreak size r depends on μ as the loop effects exist whenever $r > 0$. Here we present an exact calculation of the dependence based on a standard tree ansatz for the random SFNs [10, 15, 34, 35]. To this end, we consider the probability q_l that a node l links away from the seed is eventually infected. For simplicity, we assume $k_m \geq n-2$, which does not affect the main results. Then q_l evolves

TABLE I. Scaling exponents describing tricritical properties of the GEP on random SFNs.

	β_t	β_c	ϕ
$\alpha > 5$	$\frac{1}{2}$	1	$\frac{1}{2}$
$4 < \alpha < 5$	$\frac{1}{\alpha-3}$	1	$\frac{\alpha-4}{\alpha-3}$
$3 < \alpha < 4$	1	$\frac{1}{\alpha-3}$	$4 - \alpha$
$2 < \alpha < 3$	$\frac{4-\alpha}{3-\alpha}$	$\frac{1}{3-\alpha}$	$\frac{1}{\alpha-2}$

by a map $q_{l+1} = f(q_l)$ defined as

$$f(q_l) \equiv 1 - \sum_{k=k_m}^{\infty} p'_k \left[\sum_{m=0}^{k-1} \binom{k-1}{m} (1-\lambda)^{\min[m,n-1]} \right.$$
$$\left. \times (1-\mu)^{\max[0,m-n+1]} q_l^m (1-q_l)^{k-1-m} \right], \quad (3)$$

where $p'_k \equiv k p_k / \langle k \rangle$ is the degree distribution of a node at the end of a path, weighted by k because higher-degree nodes are more likely to be connected. Each summand gives the probability that the node survives m infection attempts from its neighbors. If q_l saturates to a stable fixed point q as $l \to \infty$, r is similarly obtained as

$$r = 1 - \sum_{k=k_m}^{\infty} p_k \left[\sum_{m=0}^{k} \binom{k}{m} (1-\lambda)^{\min[m,n-1]} \right.$$
$$\left. \times (1-\mu)^{\max[0,m-n+1]} q_l^m (1-q_l)^{k-m} \right], \quad (4)$$

where p_k appears instead of p'_k because all nodes have equal weights regardless of k in the definition of r. For any choice of parameters, Eqs. (3) and (4) provide an exact, albeit implicit, solution for r. Examples of the exact results are shown in Fig. 1(b) for the GEP with $n = 3$ on the SFNs with $k_m = 4$.

Conditions for MOTs. — A MOT occurs at $\lambda = \lambda_c$ when it coincides with a discontinuous jump of r. Since Eq. (4) implies $r \simeq \langle k \rangle \lambda q$, the transitions of r should be of the same type as those of q. The latter are encoded in the small-q_l expansion of Eq. (3), which for noninteger α is given by (see Appendix B for the detailed derivation)

$$f(q_l) = \frac{\zeta_{\alpha-2,k_m} - \zeta_{\alpha-1,k_m}}{\zeta_{\alpha-1,k_m}} \lambda q_l$$
$$+ \left(\frac{\zeta_{\alpha-3,k_m} - 3\zeta_{\alpha-2,k_m}}{2\zeta_{\alpha-1,k_m}} + 1 \right) g_{2,n}(\lambda,\mu) q_l^2$$
$$+ \frac{\Gamma(2-\alpha)}{\zeta_{\alpha-1,k_m}} g_{\alpha-2,n}(\lambda,\mu) q_l^{\alpha-2} + O\left(q_l^{\min[3,\alpha-1]} \right), \quad (5)$$

where Γ is the gamma function, and $g_{s,n}$ is defined as

$$g_{s,n}(\lambda,\mu) \equiv \left(\frac{1-\lambda}{1-\mu} \right)^{n-1} \left\{ -\mu^s + \sum_{m=0}^{n-2} \binom{m-1-s}{m} \right.$$
$$\left. \times (1-\mu)^m \left[1 - \left(\frac{1-\mu}{1-\lambda} \right)^{n-1-m} \right] \right\}. \quad (6)$$

Here q_l^j with an integer j corresponds to the contribution from j neighbors, while $q_l^{\alpha-2}$ stems from the hubs. We note that the latter gets an extra factor of $\ln q_l$ for the special cases where α is an integer, which leads to some complications (see Appendix C for more detail). By standard methods, one observes that $q = 0$ is stable (unstable) if $f'(0) < 1$ ($f'(0) > 1$) and that the sta-

ble fixed point changes continuously (discontinuously) at $f'(0) = 1$ if $f''(0) < 0$ ($f''(0) > 0$) there. Whether the map (3) meets these criteria is determined by the signs of the two lowest-order terms of Eq. (5). Then it is easy to check that the transition between $r = 0$ and $r > 0$ occurs at $\lambda = \lambda_c$ given by Eq. (2). Moreover, the transition of r is continuous (discontinuous) if $\mu < \mu_t$ ($\mu > \mu_t$), where $\mu_t \in [0,1]$ is a solution of

$$g_{\min[2,\alpha-2],n}(\lambda_c,\mu_t) = 0 \quad (7)$$

for any noninteger $\alpha > 2$. In Fig. 1(c), we show examples of λ_c and μ_t on the SFNs with $k_m = 4$ satisfying this equation. The solvability of Eq. (7) has the following implications:

(i) If $\alpha > 4$, for $n = 2$ the solution is $\mu_t = \frac{\lambda_c}{1-\lambda_c}$, which depends on α only through λ_c. This is because the transition type is determined by the sign of q_l^2 in Eq. (5), which is a two-neighbor effect. On the other hand, for $n \geq 3$ there is no solution because $g_{2,n}(\lambda_c,\mu_t) = -\lambda_c^2 < 0$; in other words, $f''(0) < 0$ always holds, so the transition of r is always continuous. Here μ comes into play only for three-or-more infected neighbors, so it cannot affect the sign of q_l^2.

(ii) If $3 < \alpha < 4$, Eq. (7) is explicitly dependent on α, reflecting the dominance of the hub-induced $q_l^{\alpha-2}$ term. Here the solution exists for any $n \geq 2$, implying that cooperation requiring a large number of neighbors can still create a large-scale avalanche at λ_c because many infection pathways converge at the hubs. We note that μ_t obtained from Eq. (7), depending on k_m, can still be larger than 1 and thus impossible to achieve, as shown for $k_m = 4$ in Fig. 1(c).

(iii) If $2 < \alpha < 3$, for any $n \geq 2$, $\mu_t = 0$ is the only solution. This captures $\lim_{\lambda \downarrow 0} r$ being positive (zero) for $\mu > 0$ ($\mu = 0$); in other words, there are so many infection pathways crossing at the hubs that, regardless of n, μ alone can induce an outbreak with little aid from λ.

Based on these results, one can interpret the transition behaviors of the GEP with $n = 3$ on the SFNs with $k_m = 4$ illustrated in Fig. 1(b). For $\alpha = 3.5$, both continuous and discontinuous transitions of r are possible at $\lambda_c \approx 0.104$ with the boundary at $\mu_t \approx 0.371$, whereas for $\alpha = 4.5$ (see the inset for a magnified view) r undergoes a continuous transition belonging to the bond percolation universality class ($\beta_c = 1$) at $\lambda_c \approx 0.203$ even in the extreme case $\mu = 1$. Notably, there is a secondary discontinuous transition (marked by dotted vertical lines) at $\lambda > \lambda_c$, whose possibility is not excluded by our argument. This phenomenon seems to be related to the double phase transitions reported in [23] and will be discussed in detail elsewhere [37].

Tricritical behaviors for $\alpha > 3$. — For small and positive ϵ_λ, a Taylor expansion of Eq. (5) about $(\lambda,\mu) =$
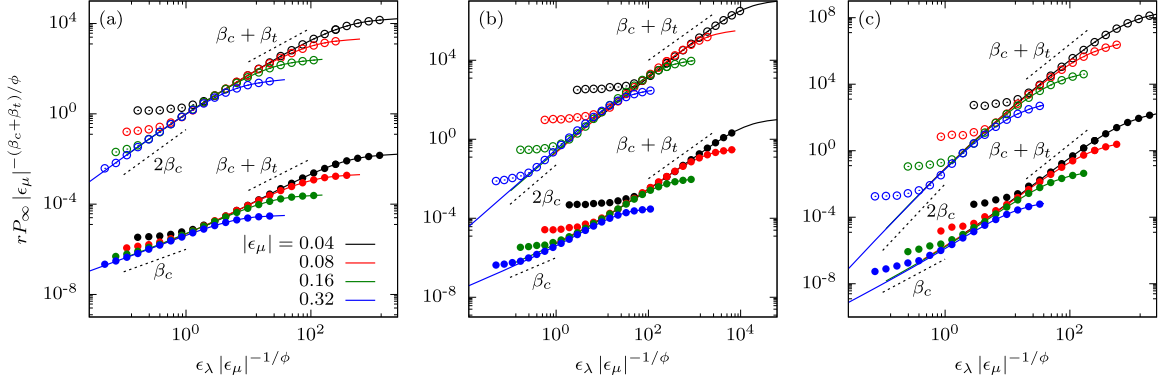
FIG. 2. The near-TCP crossover behaviors for $n = 2$ described by Eq. (9). The lines are obtained from the fixed points of Eq. (5), and the symbols are simulation results obtained using 10^5 SFNs with $N = 10^7$ and $k_m = 4$. The upper (lower) data correspond to the $\epsilon_\mu < 0$ ($\epsilon_\mu > 0$) regime with (a) $\alpha = 5.5$, (b) $\alpha = 4.5$, and (c) $\alpha = 3.5$. To remove overlaps, all data for $\epsilon_\mu < 0$ have been divided by 10^6. All plots use the same values of $|\epsilon_\mu|$.

(λ_c, μ_t) yields

$$r \sim q \sim \begin{cases} (\epsilon_\lambda/|\epsilon_\mu|)^{\beta_c} & \text{if } |\epsilon_\mu| \gg \epsilon_\lambda^\phi, \ \epsilon_\mu < 0, \\ \epsilon_\lambda^{\beta_t} & \text{if } |\epsilon_\mu| \ll \epsilon_\lambda^\phi, \\ \epsilon_\mu^{\beta_t/\phi} & \text{if } |\epsilon_\mu| \gg \epsilon_\lambda^\phi, \ \epsilon_\mu > 0, \end{cases} \tag{8}$$

where $\epsilon_\mu \equiv (\mu - \mu_t)/\mu_t$, the exponents β_c and β_t are shown in Table I as well as Fig. 1(d), and $\phi = 1 - \beta_t/\beta_c$. The new exponent β_t clearly reveals the unique critical behavior of r near the TCP $(\lambda, \mu) = (\lambda_c, \mu_t)$. The exponent ϕ, which governs the crossover between different scaling regimes, exhibits nonmonotonic behaviors that reflects the changing role of the hubs in different ranges of α (see Fig. 1(d)). As α is reduced toward 4, the avalanche driven by the two-neighbor infections gives way to the many-neighbor effects of hubs more quickly (see also Appendix D), making large-scale avalanches more difficult. In this regime, decreasing α broadens the tricritical regime described by the second case of Eq. (8). In contrast, for $3 < \alpha < 4$, decreasing α strengthens the hub-driven avalanche and makes r more sensitive to ϵ_μ. Thus, in this case, the tricritical regime gets narrower with smaller α.

To numerically verify the scaling exponents derived above, we present the scaling form for $r P_\infty$, which converges to the average fraction of **R**-nodes, $\langle R \rangle/N$, readily obtained using random SFNs of N nodes (see Appendix A for more detail) in the $N \to \infty$ limit. The scaling form is given by

$$r P_\infty = \lim_{N \to \infty} \frac{\langle R \rangle}{N} = |\epsilon_\mu|^{(\beta_t + \beta_c)/\phi} f_\pm \left(\epsilon_\lambda |\epsilon_\mu|^{-1/\phi} \right), \tag{9}$$

where f_+ (f_-) is the scaling function for $\epsilon_\mu > 0$ ($\epsilon_\mu < 0$). As shown in Fig. 2, there is a good agreement between the theory and the numerics, despite deviations due to the finite-size effects for small $|\epsilon_\lambda|$ and $|\epsilon_\mu|$.

Scaling behaviors for $2 < \alpha < 3$. — As discussed above and illustrated in Figs. 3(a) and 3(b) (the latter provid-
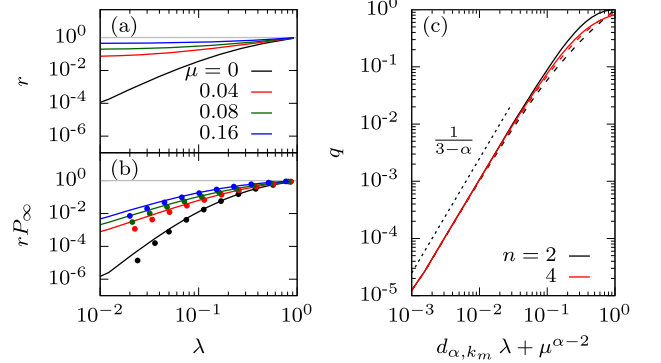

FIG. 3. (a) Scaling behaviors of the outbreak size r on the SFNs with $\alpha = 2.5$ and $k_m = 4$. (b) Comparison between the asymptotic values of $r P_\infty$ (solid lines) predicted by the fixed points of Eq. (5) and the corresponding finite-size observable $\langle R \rangle/N$ (symbols) numerically obtained from 10^5 networks with $N = 10^6$. Both (a) and (b) use $n = 2$ and the same values of μ. (c) Data collapse of q with respect to $d_{\alpha, k_m} \lambda + \mu^{\alpha-2}$, as predicted by Eq. (10). The solid (dashed) lines correspond to $\lambda = 0$ ($\mu = 0$).

ing a numerical verification), in this case the endemic phase is simply absent and $\lambda_c = \mu_t = 0$. While it would be misleading to call the point a TCP, one can still identify universal scaling behaviors and the crossover between them from the leading-order terms of Eq. (5), which gives

$$q \sim \left(d_{\alpha, k_m} \lambda + \mu^{\alpha-2} \right)^{1/(3-\alpha)}, \tag{10}$$

as illustrated in Fig. 3(c). For $\mu = 0$, the above equation and $r \sim \lambda q$ from Eq. (4) implies $r \sim \lambda^{\beta_t}$ with $\beta_t = \frac{4-\alpha}{3-\alpha}$. Moreover, since the positive limiting values of q and r as λ decreases to zero become clear only for $\mu \gg \lambda^{\frac{1}{\alpha-2}}$, we can also write $\phi = \frac{1}{2-\alpha}$ to describe the crossover. The behaviors of β_t and ϕ for $2 < \alpha < 3$ shown in Table I and Fig. 1(c) should be understood in this vein.

Summary. — We examined the effects of the degree exponent α on the endemic-to-epidemic phase transitions

of the GEP on uncorrelated random SFNs. All results, based on the tree ansatz (3), are exact and in good agreement with the numerics beyond the regime of strong finite-size effects. It is found that the hub-driven MOTs occur only for $\alpha < 4$, which is manifest in the impossibility of such transitions for $\alpha > 4$ at high cooperation thresholds ($n \geq 3$) and the changing sign of $d\phi/d\alpha$ at $\alpha = 4$. Moreover, for $2 < \alpha < 3$, an epidemic outbreak becomes possible whenever either λ or μ is nonzero via hub infections. This is a distinct phenomenon of behavioral epidemics not observed in cooperative co-infections on the random SFNs [24], which suggests a fundamental difference between the two in typical social networks with $2 < \alpha < 3$. These findings confirm and elaborate on the significance of long-range interactions in mixed-order transitions claimed in previous studies [3, 5, 16–18]. They also lay the framework for understanding the tricritical percolation, mostly studied in homogeneous media [11–15, 38, 39], in a broader context including heterogeneous structures. There still remain the questions of whether the presence of many short loops, degree correlations between neighboring nodes, and the community structure of realistic social networks lead to significant changes. Moreover, the nature of the finite-size effects remains to be clarified.

Appendix A: Generation of scale-free networks

In our simulations of the GEP, we randomly generated the SFNs according to the following three-step scheme.

Step 1. Depending on the value of α, fix the maximum degree as

$$k_{\max} = \begin{cases} N - 1 & \text{if } \alpha \geq 3, \\ \lfloor \sqrt{N} \rfloor & \text{if } 2 < \alpha < 3.t \end{cases} \tag{A1}$$

This ensures that the degrees of adjacent nodes are uncorrelated [40].

Step 2. Given the degree distribution

$$p_k = \frac{k^{-\alpha}}{\sum_{k'=k_m}^{k_{\max}} k'^{-\alpha}}, \tag{A2}$$

generate a degree sequence *deterministically* so that the number of nodes with degree k, denoted by N_k, satisfies

$$\left\lfloor N \sum_{k'>k} p_{k'} \right\rfloor = \sum_{k'>k} N_{k'}, \tag{A3}$$

for every integer $k \in [k_m, k_{\max}]$. This method, used in [41], reduces the noise stemming from the sample-to-sample fluctuations of the degree sequence at finite N.

Step 3. Randomly connect the nodes according to the given degree sequence, avoiding the creation of self-loops and multiple links between the same pair of nodes.

Appendix B: Derivation of Eq. (5)

We first rewrite Eq. (3) of the main text as

$$
f(q_l) = 1 - \sum_{k=k_m}^{\infty} p_k' \left[\sum_{m=0}^{n-1} \binom{k-1}{m} (1-\lambda)^m q_l^m (1-q_l)^{k-1-m} + \sum_{m=n}^{k-1} \binom{k-1}{m} (1-\lambda)^{n-1} (1-\mu)^{m-n+1} q_l^m (1-q_l)^{k-1-m} \right]
$$

$$
= 1 - \sum_{k=k_m}^{\infty} p_k' \left\{ \left(\frac{1-\lambda}{1-\mu}\right)^{n-1} (1-\mu q_l)^{k-1} + \sum_{m=0}^{n-2} \binom{k-1}{m} (1-\lambda)^m \left[1 - \left(\frac{1-\lambda}{1-\mu}\right)^{n-m-1} \right] q_l^m (1-q_l)^{k-1-m} \right\},
\tag{B1}
$$

whose validity can be easily shown by the binomial expansion of $(1-\mu q_l)^{k-1}$. Using a notation for the *Lerch transcendent*

$$
\Phi_{s,v}(z) \equiv \sum_{i=0}^{\infty} \frac{z^i}{(v+i)^s},
\tag{B2}
$$

we can calculate the summations over k in Eq. (B1) to obtain

$$
f(q_l) = 1 - \frac{1}{\zeta_{\alpha-1,k_m}} \left(\frac{1-\lambda}{1-\mu}\right)^{n-1} (1-\mu q_l)^{k_m-1} \Phi_{\alpha-1,k_m}(1-\mu q_l)
$$

$$
- \frac{1}{\zeta_{\alpha-1,k_m}} \sum_{m=0}^{n-2} \frac{(1-\lambda)^m}{m!} \left[1 - \left(\frac{1-\lambda}{1-\mu}\right)^{n-m-1} \right] (-q_l)^m \frac{d^m}{dq_l^m} \left[(1-q_l)^{k_m-1} \Phi_{\alpha-1,k_m}(1-q_l) \right].
\tag{B3}
$$

In order to expand the rhs of Eq. (B3) with respect to q_l, we note that the Lerch transcendent has a series expansion [42]

$$
\Phi_{s,v}(z) = z^{-v} \sum_{i=0}^{\infty} \zeta_{s-i,v} \frac{(\ln z)^i}{i!} + z^{-v} \Gamma(1-s)(-\ln z)^{s-1}
\tag{B4}
$$

for any complex z with $|\ln z| < 2\pi$ and for real numbers s and v satisfying $s \neq 1, 2, 3, \dots$ and $v \neq 0, -1, -2, \dots$. Taking advantage of the generating function

$$
[\ln(1-x)]^i = (-1)^i \cdot i! \cdot \sum_{j=i}^{\infty} \begin{bmatrix} j \\ i \end{bmatrix} \frac{x^j}{j!}
\tag{B5}
$$

for the *unsigned Stirling numbers of the first kind* $\begin{bmatrix} j \\ i \end{bmatrix}$, we can derive a useful relation

$$
\frac{[\ln(1-x)]^i}{1-x} = -\frac{1}{i+1} \frac{d}{dx} [\ln(1-x)]^{i+1} = (-1)^i \cdot i! \cdot \sum_{j=i+1}^{\infty} \begin{bmatrix} j \\ i+1 \end{bmatrix} \frac{x^{j-1}}{(j-1)!}.
\tag{B6}
$$

This in turn can be used to rewrite Eq. (B4) in a more convenient form

$$
(1-x)^{v-1} \Phi_{s,v}(1-x) = \sum_{j=1}^{\infty} \left\{ \sum_{i=0}^{j-1} (-1)^i \begin{bmatrix} j \\ i+1 \end{bmatrix} \zeta_{s-i,v} \right\} \frac{x^{j-1}}{(j-1)!} + \frac{\Gamma(1-s)}{\zeta_{s,v}} x^{s-1} [1 + O(x)]
$$

$$
= \sum_{j=0}^{\infty} \left\{ \sum_{i=1}^{j+1} (-1)^{i+1} \begin{bmatrix} j+1 \\ i \end{bmatrix} \zeta_{s-i+1,v} \right\} \frac{x^j}{j!} + \frac{\Gamma(1-s)}{\zeta_{s,v}} \left[x^{s-1} + O(x^s) \right],
\tag{B7}
$$

where the second equality is obtained by the change of variables $j \to j+1$ and $i \to i-1$. Using the above expansion in Eq. (B3), a tedious but straightforward calculation yields

$$f(q_l) = \sum_{j=1}^{\infty} \left\{ \sum_{i=1}^{j+1} \frac{(-1)^{i+1}}{j!} \begin{bmatrix} j+1 \\ i \end{bmatrix} \frac{\zeta_{\alpha-i,k_m}}{\zeta_{\alpha-1,k_m}} \right\} \left(\frac{1-\lambda}{1-\mu}\right)^{n-1} \left\{ \sum_{m=0}^{n-2} \binom{m-1-j}{m} (1-\mu)^m \left[1 - \left(\frac{1-\mu}{1-\lambda}\right)^{n-1-m}\right] - \mu^j \right\} q_l^j$$
$$+ \frac{\Gamma(2-\alpha)}{\zeta_{\alpha-1,k_m}} \left(\frac{1-\lambda}{1-\mu}\right)^{n-1} \left\{ \sum_{m=0}^{n-2} \binom{m+1-\alpha}{m} (1-\mu)^m \left[1 - \left(\frac{1-\mu}{1-\lambda}\right)^{n-1-m}\right] - \mu^{\alpha-2} \right\} \left[q_l^{\alpha-2} + O\left(q_l^{\alpha-1}\right)\right]. \quad \text{(B8)}$$

We directly obtain Eq. (3) of the main text from this result by defining $g_{s,n}(\lambda, \mu)$ as in Eq. (6) of the main text.

Appendix C: Phase transitions at integer degree exponents

If the degree exponent α is an integer, the epidemic outbreaks and their associated critical phenomena are governed by the behavior of $\Phi_{s,v}(z)$ near $z=1$ for a positive integer s. The relevant series expansion is given by [42]

$$\Phi_{s,v}(z) \equiv z^{-v} \sum_{n=0}^{\infty} \tilde{\zeta}_{s-n,v} \frac{(\ln z)^n}{n!} + z^{-v} \left[\psi(s) - \psi(v) - \ln(-\ln z)\right] \frac{(\ln z)^{s-1}}{(s-1)!} \quad \text{(C1)}$$

for $|\ln z| < 2\pi$ and $v \neq 0, -1, -2, \ldots$, where we have introduced the notations

$$\tilde{\zeta}_{s,v} \equiv \begin{cases} \zeta_{s,v} & \text{if } s \geq 2, \\ 0 & \text{if } s = 1 \end{cases} \quad \text{(C2)}$$

and $\psi(s) \equiv \Gamma'(s)/\Gamma(s)$ for the digamma function. Using Eq. (B5), we can recast the above expansion into a more convenient form

$$(1-x)^{v-1} \Phi_{s,v}(1-x) = \sum_{j=0}^{\infty} \left\{ \sum_{i=1}^{j+1} (-1)^{i+1} \begin{bmatrix} j+1 \\ i \end{bmatrix} \tilde{\zeta}_{s-i+1,v} \right\} \frac{x^j}{j!} - \frac{(-1)^{s-1}}{(s-1)!} \left\{ x^{s-1} \ln x + [\psi(v) - \psi(s)] x^{s-1} \right\} + O(x^s).$$
$$\text{(C3)}$$

Based on this formula, we can expand the rhs of Eq. (B3) as

$$f(q_l) = \sum_{j=1}^{\infty} \left\{ \sum_{i=1}^{j+1} \frac{(-1)^{i+1}}{j!} \begin{bmatrix} j+1 \\ i \end{bmatrix} \frac{\tilde{\zeta}_{\alpha-i,k_m}}{\zeta_{\alpha-1,k_m}} \right\} g_{j,n}(\lambda, \mu) q_l^j - \frac{(-1)^{\alpha-2}}{\zeta_{\alpha-1,k_m}(\alpha-2)!} g_{\alpha-2,n}(\lambda, \mu) q_l^{\alpha-2} \ln q_l$$
$$- \frac{(-1)^{\alpha-2}}{\zeta_{\alpha-1,k_m}(\alpha-2)!} \left[[\psi(k_m) - \psi(\alpha-1)] g_{\alpha-2,n}(\lambda, \mu) - \left(\frac{1-\lambda}{1-\mu}\right)^{n-1} \left\{ \mu^{\alpha-2} \ln \mu \right. \right.$$
$$\left. \left. - \sum_{m=0}^{\min[\alpha,n]-2} (1-\mu)^m \left[1 - \left(\frac{1-\mu}{1-\lambda}\right)^{n-1-m}\right] \binom{m+1-\alpha}{m} [\psi(\alpha-1) - \psi(\alpha-1-m)] \right\} \right] q_l^{\alpha-2} + O\left(q_l^{\alpha-1} \ln q_l\right),$$
$$\text{(C4)}$$

where we have used $g_{s,n}(\lambda, \mu)$ defined in Eq. (6) of the main text. The main difference between Eq. (5) of the main text and Eq. (C4) lies in the presence of $q^{\alpha-2} \ln q$ in the latter, which is always lower-order than $q^{\alpha-2}$. If $\alpha > 5$, the term is simply irrelevant to epidemic outbreaks. If $\alpha \in \{3, 4, 5\}$, the logarithmic correction has nontrivial effects on the transition behaviors, as discussed case by case below (see Table S1 for a summary).

Case of $\alpha = 5$: here the lowest-order terms of Eq. (C4) are given by

$$f(q_l) = \frac{\zeta_{3,k_m} - \zeta_{4,k_m}}{\zeta_{4,k_m}} \lambda q_l + \frac{\zeta_{2,k_m} - 3\zeta_{3,k_m} + 2\zeta_{4,k_m}}{2\zeta_{4,k_m}} g_{2,n}(\lambda, \mu) \, q_l^2 + \frac{g_{3,n}(\lambda, \mu)}{6\zeta_{4,k_m}} q_l^3 \ln q_l + O(q_l^3), \tag{C5}$$

whose form is similar to the corresponding recursive relation for a non-integer $\alpha > 4$. Based on the same arguments described in the main text, the epidemic threshold is obtained as $\lambda_c = \zeta_{4,k_m}/(\zeta_{3,k_m} - \zeta_{4,k_m})$, and the TCP satisfies $g_{2,n}(\lambda_c, \mu_t) = 0$, which has a physical solution $\mu_t = \lambda_c/(1 - \lambda_c) \in (0, 1)$ for $n = 2$ and sufficiently large k_m. Near the TCP, we can approximate the above equation as

$$\frac{dq_l}{dl} \simeq \epsilon_\lambda q_l + c_{\alpha,k_m} \epsilon_\mu q_l^2 - c'_{\alpha,k_m} q_l^3 |\ln q_l|, \tag{C6}$$

where c_{α,k_m} and c'_{α,k_m} are positive coefficients. Thus the behavior of the outbreak size in this regime satisfies

$$r \sim q \sim \begin{cases} \epsilon_\lambda/|\epsilon_\mu| & \text{if } \epsilon_\mu < 0, \ |\epsilon_\mu| \gg |\epsilon_\lambda \ln \epsilon_\lambda|^{1/2}, \\ |\epsilon_\lambda/\ln \epsilon_\lambda|^{1/2} & \text{if } |\epsilon_\mu| \ll |\epsilon_\lambda \ln \epsilon_\lambda|^{1/2}, \\ \epsilon_\mu/|\ln \epsilon_\mu| & \text{if } \epsilon_\mu > 0, \ |\epsilon_\mu| \gg |\epsilon_\lambda \ln \epsilon_\lambda|^{1/2}. \end{cases} \tag{C7}$$

Case of $\alpha = 4$: here the lowest-order terms of Eq. (C4) are obtained as

$$
\begin{aligned}
f(q_l) = {} & \frac{\zeta_{2,k_m} - \zeta_{3,k_m}}{\zeta_{3,k_m}} \lambda q_l - \frac{g_{2,n}(\lambda, \mu)}{2\zeta_{3,k_m}} q_l^2 \ln q_l \\
& - \frac{1}{2\zeta_{3,k_m}} \Bigg[[3\zeta_{2,k_m} - 2\zeta_{3,k_m} + \psi(k_m) - \psi(3)] \, g_{2,n}(\lambda, \mu) - \left(\frac{1-\lambda}{1-\mu}\right)^{n-1} \Bigg\{ \mu^2 \ln \mu \\
& - \sum_{m=0}^{\min[4,n]-2} (1-\mu)^m \left[1 - \left(\frac{1-\mu}{1-\lambda}\right)^{n-1-m}\right] \binom{m-3}{m} [\psi(3) - \psi(3-m)] \Bigg\} \Bigg] q_l^2 + O(q_l^3 \ln q_l), \tag{C8}
\end{aligned}
$$

which implies that the epidemic threshold is at $\lambda_c = \zeta_{3,k_m}/(\zeta_{2,k_m} - \zeta_{3,k_m})$ and that the TCP satisfies $g_{2,n}(\lambda_c, \mu_t) = 0$. As was the case for $\alpha > 4$, the TCP exists only for $n = 2$ and sufficiently large k_m. The near-TCP properties are described by

$$\frac{dq_l}{dl} \simeq \epsilon_\lambda q_l + c_{\alpha,k_m} \epsilon_\mu q_l^2 |\ln q_l| - c'_{\alpha,k_m} q_l^2, \tag{C9}$$

for positive coefficients c_{α,k_m} and c'_{α,k_m}. Thus the outbreak size in this regime obeys

$$r \sim q \sim \begin{cases} \epsilon_\lambda/|\epsilon_\mu \ln(\epsilon_\lambda/|\epsilon_\mu|)| & \text{if } \epsilon_\mu < 0, \ |\epsilon_\mu| \gg |\ln \epsilon_\lambda|^{-1}, \\ \epsilon_\lambda & \text{if } |\epsilon_\mu| \ll |\ln \epsilon_\lambda|^{-1}, \\ e^{-c'_{\alpha,k_m}/(c_{\alpha,k_m}\epsilon_\mu)} & \text{if } \epsilon_\mu > 0, \ |\epsilon_\mu| \gg |\ln \epsilon_\lambda|^{-1}. \end{cases} \tag{C10}$$

Case of $\alpha = 3$: here the lowest-order terms of Eq. (C4) are given by

$$
\begin{aligned}
f(q_l) = {} & -\frac{1}{\zeta_{2,k_m}} \lambda q_l \ln q_l - \frac{1}{\zeta_{2,k_m}} \Bigg[[\zeta_{2,k_m} + \psi(k_m) - \psi(2)] \lambda + \left(\frac{1-\lambda}{1-\mu}\right)^{n-1} \Bigg\{ \mu \ln \mu \\
& - \sum_{m=0}^{\min[3,n]-2} (1-\mu)^m \left[1 - \left(\frac{1-\mu}{1-\lambda}\right)^{n-1-m}\right] \binom{m-2}{m} [\psi(2) - \psi(2-m)] \Bigg\} \Bigg] q_l + O(q_l^2), \tag{C11}
\end{aligned}
$$

which has a nonzero stable fixed point whenever $\lambda > 0$. Thus the epidemic threshold vanishes ($\lambda_c = 0$), and the sign

TABLE S1. Scaling exponents describing tricritical properties of the GEP (if TCPs exist) on random SFNs for integer degree exponents α.

	$r \sim \epsilon_\lambda^{\beta_t}$	$P_\infty \sim \epsilon_\lambda^{\beta_c}$	$\epsilon_\mu \sim \epsilon_\lambda^{\phi}$
$\alpha = 5$	$|\epsilon_\lambda / \ln \epsilon_\lambda|^{1/2}$	ϵ_λ	$|\epsilon_\lambda \ln \epsilon_\lambda|^{1/2}$
$\alpha = 4$	ϵ_λ	$|\epsilon_\lambda / \ln \epsilon_\lambda|$	$|\ln \epsilon_\lambda|^{-1}$
$\alpha = 3$	λ^0	$\lambda e^{-c/\lambda}$	λ

of the q_l term is positive (negative) if μ is greater (less) than μ_t satisfying

$$\mu_t \ln \mu_t = \sum_{m=0}^{\min[3,n]-2} (1 - \mu_t)^m \left[1 - (1 - \mu_t)^{n-1-m} \right] \binom{m-2}{m} [\psi(2) - \psi(2-m)]. \tag{C12}$$

We note that μ_t obtained from the above equation is in general not equal to $\lim_{\alpha \downarrow 3} \mu_t$ obtained from Eq. (7) of the main text. If $\mu < \mu_t$, the transition behaviors are described by the approximate formula

$$\frac{dq_l}{dl} \simeq c_{\alpha,k_m} \lambda q_l |\ln q_l| + \left(c'_{\alpha,k_m} \epsilon_\mu - c''_{\alpha,k_m} \lambda \right) q_l, \tag{C13}$$

where c_{α,k_m}, c'_{α,k_m}, and c''_{α,k_m} are positive coefficients. In this case, the outbreak size satisfies

$$r \sim \lambda q \sim \lambda \, e^{\left(c'_{\alpha,k_m} \epsilon_\mu - c''_{\alpha,k_m} \lambda \right)/(c_{\alpha,k_m} \lambda)}. \tag{C14}$$

As ϵ_μ approaches zero so that $|\epsilon_\mu| \ll \lambda$ (which can be represented as $\phi = 1$), r abruptly becomes nonzero for an arbitrary positive value of λ. In contrast to the other cases, here r can be already nonzero at $\lambda = \lambda_c$ and $\mu = \mu_t$ in a manner analogous to a discontinuous transition.

Appendix D: Relevant length scales

Here we show that one can understand the near-TCP crossover behaviors for $\alpha > 3$ as originating from two competing length scales associated with ϵ_λ and ϵ_μ. To this end, using $dq_l/dl \simeq q_{l+1} - q_l$, we expand Eq. (5) of the main text about the TCP to write

$$\frac{dq_l}{dl} \simeq \epsilon_\lambda q_l + c_{\alpha,k_m} \epsilon_\mu q_l^{1+1/\beta_c} - c'_{\alpha,k_m} q_l^{1+1/\beta_t}, \tag{D1}$$

where c_{α,k_m} and c'_{α,k_m} are positive coefficients, and the exponents β_c and β_t have the values listed in Table I of the main text. This equation remains invariant under the spatial rescaling $l \to bl$ if the other variables rescale as

$$q_l \to b^{-\beta_t} q_{bl}, \quad \epsilon_\lambda \to b^{-1} \epsilon_\lambda, \quad \epsilon_\mu \to b^{-\phi} \epsilon_\mu. \tag{D2}$$

The scale invariance suggests the presence of the length scales

$$l_\lambda \sim |\epsilon_\lambda|^{-1}, \quad l_\mu \sim |\epsilon_\mu|^{-1/\phi}. \tag{D3}$$

One can directly observe l_λ and l_μ by examining how dq_l/dl changes over different layers for $\epsilon_\lambda > 0$ and $\epsilon_\mu > 0$. According to Eq. (D1), in this regime the derivative shows an exponential decay $dq_l/dl \sim e^{-l/\tau}$ towards saturation, as illustrated in the inset of Fig. S1. For $\epsilon_\lambda \gg \epsilon_\mu^{1/\phi}$, the first and the third terms of Eq. (D1) always stay dominant,
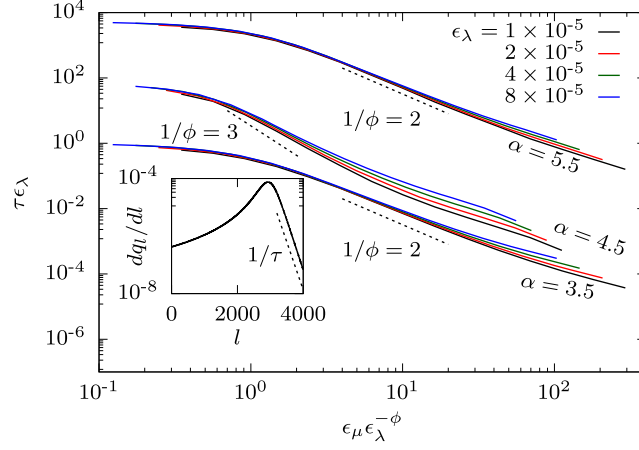
FIG. S1. The crossover behavior of the characteristic length scale τ of the GEP with $n = 2$ shown in Eq. (D4). To remove overlaps, the values of $\tau\epsilon_\lambda$ for $\alpha = 4.5$ (5.5) have been multiplied by 10^2 (10^4). (Inset) The l-dependence of dq_l/dl governed by Eq. (D1) on SF networks with $\alpha = 4.5$ and $k_m = 4$ at $\epsilon_\lambda = 10^{-5}$ and $\epsilon_\mu = 5\epsilon_\lambda^\phi$. The final exponential decay determines τ.
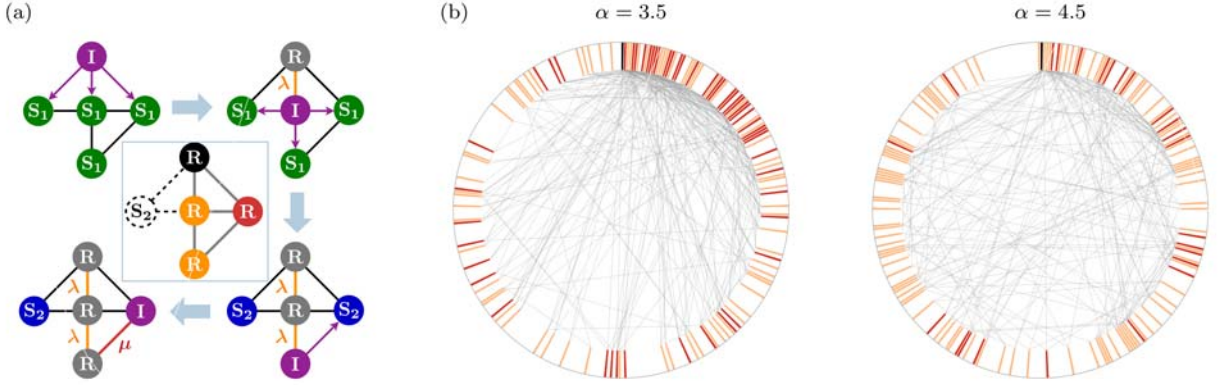

FIG. S2. Examples of the GEP with $n = 3$. (a) Entire dynamics on a five-node network. Each thick arrow represents a time step. Central box: in the final state, the seed is colored black, the nodes infected with probability λ (μ) are colored orange (red), and only the links connecting the infected nodes are shown. (b) Examples of the final state of the GEP on the SFNs with $k_m = 4$ at $\lambda = \lambda_c$, and $\mu = 0.5$. The rods (both colored and white) on the boundary correspond to the nodes, aligned clockwise in the order of decreasing degree. Only the infected nodes and their mutual links are shown according to the color scheme shown in (a). Here the seed is located at the node of the highest degree (the black rod).

and the characteristic scale τ satisfies $\tau \sim \epsilon_\lambda^{-1} \sim l_\lambda$. Thus l_λ gives the length scale of a region where λ is dominant. Meanwhile, for $\epsilon_\lambda \ll \epsilon_\mu^{1/\phi}$, the second and the third terms of Eq. (D1) eventually dominate the dynamics before saturation. In this case, one observes $\tau \sim \epsilon_\mu^{-1/\phi} \sim l_\mu$, which indicates the length scale of the μ-dominant region. In this sense, the decrease (increase) of ϕ with decreasing α for $\alpha > 4$ ($3 < \alpha < 4$) can be interpreted as reflecting the decreasing (increasing) depth of the μ-dominant growth regime.

The two different scaling regimes of τ yields yet another crossover phenomenon, which is described by

$$\tau = l_\lambda\, g(l_\lambda/l_\mu) = \epsilon_\lambda^{-1}\tilde{g}(\epsilon_\lambda\epsilon_\mu^{-1/\phi}). \tag{D4}$$

In Fig. S1, we check this scaling form based on numerical solutions of Eq. (B3) for each sub-interval of $\alpha > 3$.

Appendix E: Illustrations of actual outbreaks

The importance of hubs in the MOTs for $3 < \alpha < 4$ is more directly illustrated in Fig. S2. Using the color scheme described in Fig. S2(a), each circular diagram of Fig. S2(b) shows the final state of the GEP with $n = 3$ at $\lambda = \lambda_c$ and $\mu = 0.5$ on the random SFNs with $N = 360$ nodes and $k_m = 4$. More specifically, each rod on the periphery corresponds to a node, aligned clockwise in the order of decreasing degree (nodes of equal degree are randomly ordered). The seed node (chosen to be the node of the highest degree) is black, the nodes infected in the $\mathbf{S_1}$-state are orange, and those infected in the $\mathbf{S_2}$-state are red. The uninfected nodes are left as vacancies. The links are drawn with grey lines only if they connect two infected neighbors. By comparing these two examples of epidemic outbreaks at $\alpha = 3.5$ and 4.5, it is clear that the $\mathbf{S_2} \to \mathbf{I}$ infections (red nodes) are especially frequent among the high-degree nodes in the case of $\alpha = 3.5$. This reflects the dominant role played by the hubs in the system-wide avalanche for $3 < \alpha < 4$ (note that $\mu = 0.5 > \mu_t \approx 0.371$ in this case). In contrast, for $\alpha = 4.5$, the high cooperation threshold $n = 3$ and the dominance of two-neighbor effects reduce the significance of cooperative infections among the hubs at the transition, which is bound to be purely continuous. Consequently, the nodes infected by the cooperative mechanism are more evenly distributed among different degrees in the latter case.

[1] D. Poland and H. A. Scheraga, J. Chem. Phys. **45**, 1456 (1966).
[2] Y. Kafri, D. Mukamel, and L. Peliti, Phys. Rev. Lett. **85**, 4988 (2000).
[3] A. Bar and D. Mukamel, Phys. Rev. Lett. **112**, 015701 (2014).
[4] N. Araújo, P. Grassberger, B. Kahng, K. J. Schrenk, and R. M. Ziff, Eur. Phys. J. Special Topics **223**, 2307 (2014).
[5] A. Bar and D. Mukamel, J. Stat. Mech. **2014**, P11001 (2014).
[6] D. J. Watts, Proc. Natl. Acad. Sci. USA **99**, 5766 (2002).
[7] P. L. Krapivsky, S. Redner, and D. Volovik, J. Stat. Mech. **2011**, P12003 (2011).
[8] P. S. Dodds and D. J. Watts, Phys. Rev. Lett. **92**, 218701 (2004).
[9] P. S. Dodds and D. J. Watts, J. Theor. Biol. **232**, 587 (2005).
[10] G. Bizhani, M. Paczuski, and P. Grassberger, Phys. Rev. E **86**, 011128 (2012).
[11] H.-K. Janssen, M. Müller, and O. Stenull, Phys. Rev. E **70**, 026114 (2004).
[12] H.-K. Janssen and O. Stenull, Europhys. Lett. **113**, 26005 (2016).
[13] H.-K. Janssen and O. Stenull, J. Phys. A: Math. Theor. **50**, 324002 (2017).
[14] K. Chung, Y. Baek, D. Kim, M. Ha, and H. Jeong, Phys. Rev. E **89**, 052811 (2014).
[15] K. Chung, Y. Baek, M. Ha, and H. Jeong, Phys. Rev. E **93**, 052304 (2016).
[16] W. Cai, L. Chen, F. Ghanbarnejad, and P. Grassberger, Nat. Phys. **11**, 936 (2015).
[17] P. Grassberger, L. Chen, F. Ghanbarnejad, and W. Cai, Phys. Rev. E **93**, 042316 (2016).
[18] D. Lee, W. Choi, J. Kertész, and B. Kahng, Sci. Rep. **7**, 5723 (2017).
[19] W. Choi, D. Lee, and B. Kahng, Phys. Rev. E **95**, 022304 (2017).
[20] W. Choi, D. Lee, and B. Kahng, Phys. Rev. E **95**, 062115 (2017).
[21] W. Choi, D. Lee, J. Kertész, and B. Kahng, Phys. Rev. E **98**, 012311 (2018).
[22] L. Chen, F. Ghanbarnejad, W. Cai, and P. Grassberger, Europhys. Lett. **104**, 50001 (2013).
[23] B. Min and M. S. Miguel, Sci. Rep. **8**, 10422 (2018).
[24] P.-B. Cui, F. Colaiori, and C. Castellano, Phys. Rev. E **96**, 022301 (2017).
[25] D. Centola, Science **329**, 1194 (2010).
[26] J. F. Brundage and G. D. Shanks, Emerg. Infect. Dis. **14**, 1193 (2008).
[27] A. Pawlowski, M. Jansson, M. Sköld, M. E. Rottenberg, and G. Källenius, PLOS Pathogens **8**, e1002464 (2012).
[28] R. Pastor-Satorras, C. Castellano, P. Van Mieghem, and A. Vespignani, Rev. Mod. Phys. **87**, 925 (2015).
[29] Rigorously speaking, a TCP is an endpoint of the coexistence line shared by three different phases. It is unclear whether the same is true for cooperative contagions, but we follow the casual definition of a TCP as a continuous transition point at the intersection between continuous and discontinuous transition lines.
[30] R. Cohen and S. Havlin, *Complex networks: structure, robustness and function* (Cambridge University Press, Cambridge, 2010).
[31] M. E. J. Newman, *Networks: An Introduction* (OUP Oxford, Oxford, 2010).
[32] G. Bianconi and M. Marsili, J. Stat. Mech. **2005**, P06005 (2005).
[33] S. N. Dorogovtsev, Rev. Mod. Phys. **80**, 1275 (2008).
[34] M. E. J. Newman, S. H. Strogatz, and D. J. Watts, Phys. Rev. E **64**, 026118 (2001).
[35] M. E. J. Newman, Phys. Rev. E **66**, 016128 (2002).
[36] R. Cohen, D. ben-Avraham, and S. Havlin, Phys. Rev. E **66**, 036113 (2002).

[37] Y. Baek and M. Ha, In preparation.

[38] D. Cellai, A. Lawlor, K. A. Dawson, and J. P. Gleeson, Phys. Rev. Lett. **107**, 175703 (2011).

[39] N. A. M. Araújo, J. S. Andrade, R. M. Ziff, and H. J. Herrmann, Phys. Rev. Lett. **106**, 095703 (2011).

[40] M. Catanzaro, M. Boguñá, and R. Pastor-Satorras, Phys. Rev. E **71**, 027103 (2005).

[41] J. D. Noh and H. Park, Phys. Rev. E **79**, 056115 (2009).

[42] H. Bateman, *Higher Transcendental Functions*, edited by A. Erdélyi, Vol. I (McGraw-Hill, New York, 1953).